Compressive Spatio-Temporal Forecasting of Meteorological Quantities and Photovoltaic Power

Compressive Spatio-Temporal Forecasting of Meteorological Quantities and Photovoltaic Power

Akin Tascikaraoglu, *Member, IEEE*, Borhan M. Sanandaji, *Member, IEEE*, Gianfranco Chicco, *Senior Member, IEEE*, Valeria Cocina, Filippo Spertino, *Member, IEEE*, Ozan Erdinc, *Member, IEEE*, Nikolaos G. Paterakis, *Member, IEEE*, and João P. S. Catalão, *Senior Member, IEEE*

***Abstract*—This paper presents a solar power forecasting scheme, which uses spatial and temporal time series data along with a photovoltaic (PV) power conversion model. The PV conversion model uses the forecast of three different variables, namely, irradiance on the tilted plane, ambient temperature, and wind speed, in order to estimate the power produced by a PV plant at the grid connection terminals. The forecast values are obtained using a *spatio-temporal* method that uses the data recorded from a target meteorological station as well as data of its surrounding stations. The proposed forecasting method exploits the sparsity of correlations between time series data in a collection of stations. The performance of both the PV conversion model and the spatio-temporal algorithm is evaluated using high-resolution real data recorded in various locations in Italy. Comparison with other benchmark methods illustrates that the proposed method significantly improves the solar power forecasts, particularly over short-term horizons.**

***Index Terms*—Distributed generation, Forecasting, Solar irradiance measurement, Correlated data, Time series.**

A. Tascikaraoglu is with the Department of Electrical Engineering and Computer Science, University of California, Berkeley, Berkeley 94720, CA, USA, and also with the Department of Electrical Engineering, Yildiz Technical University, Istanbul 34220, Turkey (e-mail: atasci@eecs.berkeley.edu; atasci@yildiz.edu.tr).

B. M. Sanandaji is with the Department of Electrical Engineering and Computer Science, University of California, Berkeley, Berkeley 94720, CA, USA (e-mail: sanandaji@eecs.berkeley.edu).

G. Chicco, V. Cocina, and F. Spertino are with the Power and Energy Systems Group, Energy Department, Politecnico di Torino, Turin 10129, Italy (e-mail: gianfranco.chicco@polito.it; valeria.cocina@polito.it; filippo.spertino@polito.it).

O. Erdinc is with the Department of Electrical Engineering, Yildiz Technical University, Istanbul 34220, Turkey, and also with INESC-ID, Inst. Super. Tecn., University of Lisbon, Lisbon 1049-001, Portugal (e-mail: oerdinc@yildiz.edu.tr).

N. G. Paterakis is with the Department of Electrical Engineering, Eindhoven University of Technology, Eindhoven 5600 MB, The Netherlands (e-mail: n.paterakis@tue.nl).

J. P. S. Catalão is with INESC TEC and the Faculty of Engineering, University of Porto, Porto 4200-465, Portugal, also with C-MAST, University of Beira Interior, Covilhã 6201-001, Portugal, and also with INESC-ID, Instituto Superior Técnico, University of Lisbon, Lisbon 1049-001, Portugal (e-mail: catalao@ubi.pt).

I. Introduction

A. Spatio-Temporal Forecasting

ANY WEATHER variable can be forecasted with reasonable accuracy only using its historical time series data. In order to further improve the forecast performance, spatial dependency of variables can also be used along with their temporal information. For example, weather variables such as solar irradiance, temperature, wind speed, and direction tend to show high correlations among neighboring sites. Due to availability of time series data over a large number of meteorological stations, there is a recent increasing interest in using *spatio-temporal* forecasting approaches [1], [2]. However, incorporating a large amount of data is generally challenging due to its computational costs, particularly in very short-term forecasting [3]. The trade-off between the amount of data to be included in the forecasting process and the prediction performance has to be addressed using advanced algorithms.

B. Related Work

Using spatial information in forecasting various meteorological quantities has drawn considerable attention in the last decade. A large part of the literature on spatio-temporal forecasting has been devoted to wind speed and wind power estimations. The main motivation behind such methods is as follows: the downstream wind profile is greatly influenced by the upstream wind in a region, particularly in areas having certain predominant wind patterns and directions. These strong spatial correlations can be used to improve wind speed or power forecasts using spatio-temporal wind forecasting methods. Together with the technological advances in communications, it is now possible to collect data from multiple locations with desired time samplings and then use this spatial information to improve the forecasts [1], [4]–[6].

Recently, there have been also promising results incorporating spatial information in solar forecasting methods. Photovoltaic (PV) power forecast considering correlated information of power from a number of points was studied from different points of views in the literature [7]–[9]. In order to forecast the Global Horizontal Irradiance (GHI) at ground level using spatio-temporal data, Dambreville et al. [10] used an Autoregressive (AR) approach, Licciardi et al. [11] exploited Artificial Neural Networks (ANN), where nonlinear Principal Component Analysis (PCA) was used to decrease the computational burden, and Zagouras et al. [12] considered various

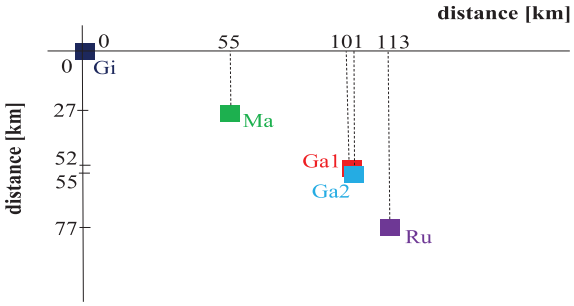

Fig. 1. Schematic map of the five considered PV plants.

models including ANN, Support Vector Machines (SVM), Genetic Algorithm (GA) and linear models. The efficiency of spatio-temporal approaches on very short-term forecasting of solar irradiance was also investigated in several studies [13], [14]. The other examples include a study on parameter shrinkage in spatio-temporal irradiance forecasting models [15] and a Hidden Markov model for variability and uncertainty forecasts in PV systems, which accounts for the effects of geographic autocorrelation [16]. Moreover, a probabilistic spatio-temporal forecasting model for wind power as well as solar power generation was presented in [17]. For a more detailed survey of spatio-temporal solar irradiance and power forecasting approaches see also [18] and [19], among others.

C. Contribution of This Work

As can be seen from the literature examples given, using temporal and spatial data might be useful in the forecasts of meteorological quantities. All of the available data are, therefore, included in the forecasting models regardless of their individual contribution on the accuracy. Instead, assuming that a sparse relational pattern usually exists among the correlations between different time series, this study proposes a spatio-temporal forecasting scheme using only these highly correlated data in the forecasting process. Exploiting such low-dimensional structures in forecasting can help improve the accuracy and decrease the computational burden. This forecasting task can be formulated as a linear inverse problem where a *block-sparse* signal is to be recovered. The proposed approach is used to forecast various variables including irradiance on the tilted plane, ambient temperature and wind speed recorded from five measuring locations in South of Italy, abbreviated as Ga1, Ga2, Gi, Ma and Ru. Figure 1 depicts the five PV plants. Each location has a meteorological station located very close to the PV system, that provides the ambient conditions for its corresponding PV plant.

The forecast of each variable is carried out by using measurements of target variables as well as two additional weather variables (wind direction and humidity) from different meteorological stations in the proposed forecasting model. The contribution of the variables from different meteorological stations on the forecasted values of target station is dynamically determined for each of the next prediction horizons, thanks to the proposed approach. In other words, contrary to the conventional time series methods in which the pre-determined input variables from each source are generally constant, the proposed algorithm gives importance to the variables from certain stations that have shown similar characteristics to the target variable in the recent prediction horizon. This adaptive feature of the proposed algorithm always provides a more up-to-date input set without realizing a time-consuming preliminary analysis for the best candidate variables and stations. Therefore, the proposed approach accomplishes better performance relative to the constant model structures. Moreover, exploiting highly-correlated data from different meteorological stations enables us to capture the permanently varying weather conditions caused by the daily, seasonal and annual meteorological cycles, which improves the forecast accuracy for particularly longer prediction times. It is also worth noting that the proposed approach does not require an analysis on the cloud cover and motions as opposed to relevant studies in solar forecasting [20]–[22]. In fact, the effect of cloud motions on the expected solar power is included in the forecasting algorithm when using spatial data. In addition to the forecasting approaches, a PV power conversion model incorporating the forecasts as inputs is presented in this study in order to estimate the output power produced by a PV plant [23].

D. Paper Organization

Section II describes the PV system and presents the PV conversion model. In Section III, the forecasting problem is formulated and the proposed forecasting method is introduced in Section IV. The proposed method is applied to measured time series data and the results are compared with real data and the benchmark models in Section V. The last section includes some concluding remarks and outlines the possible extensions.

II. Electric Power Evaluation

A. Description of the Grid-Connected PV System

For the calculations reported in this paper, the PV site Gi, located in the Northwest of the area and subject to solar irradiance with high variations due to the passage of clouds, has been considered as the target station. This permits to test the performance of the forecasting model under variable conditions. The real grid-connected PV system has a power rating of 993.6 kW_p at Standard Test Conditions (STC), global irradiance $G_{STC} = 1kW/m^2$ and cell temperature $T_{STC} = 25\,^{\circ}\mathrm{C}$. The PV arrays are placed on a metallic structure, which permits the natural air circulation, feed two centralized inverters with high efficiency (transformerless option). These inverters are slightly undersized with respect to the rated peak power, given that the 500-kVA inverter is supplied by a 552 kW_p array and the 400-kVA inverter is supplied by a 441.6 kW_p array, respectively.

The PV system is equipped with a local meteorological station, in which the measured physical quantities are the global irradiance G_{tcell} of a solar cell made of the same material as the 230 W_p poly-crystalline silicon modules with tilt angle of 30°, horizontal global irradiance of the pyranometer G_{hpyr} $[W/m^2]$, horizontal global irradiance G_{hcell} of the two solar cells in crystalline silicon on the horizontal plane

$[W/m^2]$, ambient temperature T_{amb} [°C], relative humidity RH and wind speed w_s $[m/s]$. For a detailed description of the experimental setup see [24].

B. Definition of the PV Conversion Model

In defining the PV conversion model, it is important to take into account the efficiencies referring to the main loss factors affecting the PV system behavior. As mentioned in [25], the main loss factors are summarized in the efficiencies defined by the following bulleted points.

- Efficiency η_{dirt} is due to losses for soiling and dirt (environmental pollution). To estimate the impact of dirt/soiling accumulation, a 10-day summer period without rain is considered. At the end of this period (10^{th} day), the horizontal solar irradiation is calculated from the pyranometer and the solar cell. At the 11^{th} day, the rain appears and naturally cleans the sensors. Finally, at the 12^{th} day (clear-sky day), the solar irradiation is calculated in such a way as to practically have the same astronomical conditions of the 10^{th} day. Therefore, differently from [26], the corresponding value of η_{dirt} for the PV plant, located in a relatively clean environment (i.e. away from mines, landfills, etc.), is determined according to the following formula

$$\eta_{dirt} = \frac{(H_{a\_rain} - H_{b\_rain})}{H_{a\_rain}} \cdot 100 \tag{1}$$

  where (H_{a_rain}) and (H_{b_rain}) are the values of the daily irradiation in two clear-sky days, one after rain (12^{th} day) and the other before rain (10^{th} day) respectively. As results, the corresponding value of η_{dirt} is in the range 0.97–0.98.
- Efficiency η_{refl} is due to reflection of the PV module glass; the corresponding value used is 0.971, taken from the PVGIS website [27].
- Efficiency η_{th} is due to the thermal losses ℓ_{th} with respect to the STC, calculated as:

$$\eta_{th} = 1 - \ell_{th} = 1 - \gamma_{th} \cdot (T_C - T_{STC}) \tag{2}$$

  where γ_{th} is the thermal coefficient of maximum power of the modules, dependent on the PV technology (for crystalline silicon $\gamma_{th} = 0.5\%/°C$); T_C is the cell temperature, which can be calculated in a first analysis as in [28] as a function of the ambient temperature T_{amb}, the cell irradiance on the tilted plane G_{tcell} and the Normal Operating Cell Temperature (NOCT) of 42–50 °C [29], [30]. This is the mean temperature in outdoor operation at G_{NOCT} = 800 W/m^2 and T_{amb} = 20 °C. In order to obtain better approximation, the solar cell temperature is calculated here by the following formula, defined in [31] from the application of neural network tools on real monitored data, also taking into account the wind speed w_s:

$$T_C = 0.943\, T_{amb} + 0.028\, G_{tcell} - 1.528\, w_s + 4.3. \tag{3}$$

  This empirical equation, derived from the U.S. sites, has a wide field of application and provides cell temperatures with adequate accuracy also in Mediterranean sites [32].
- Efficiency η_{mism} takes into account the *I-V* mismatch losses assuming that the bottleneck effect globally leads to 97% of the power rating declared by the manufacturer for all the PV modules in the PV array. This loss is a consequence of the weakest modules in the series connection inside the strings and of the weakest strings in the parallel connection inside the PV array [33].
- Efficiency η_{cable} includes the DC cable losses, with the value of 0.99 considered according to good design criteria [34].

TABLE I
INVERTER NO-LOAD POWER LOSSES AND LOSS COEFFICIENTS

PV peak power $[kW_p]$	$P_0[kW]$	c_L	$c_Q\left[(kW)^{-1}\right]$
552	1.1407	0	$3.40687 \cdot 10^{-5}$
441.6	1.0102	0	$4.06418 \cdot 10^{-5}$

On the basis of the previous efficiencies, the available power at the maximum power point is achieved by [23]:

$$P_{mpp} = P_{rated}\,(G_{tcell} - G_{lim})\,\eta_{dirt}\eta_{refl}\eta_{th}\eta_{mism}\eta_{cable} \tag{4}$$

where G_{lim} is the irradiance limit below which the output is vanishing (the limit 17.7 W/m^2 is assumed for the specific polycrystalline silicon module used, determined by interpolation of the points found in the module data sheet). Finally, considering the efficiency η_{MPPT} of the maximum power point tracker, and thanks to the model of the power conditioning unit for grid connection, the AC power injected into the grid is calculated as [28]:

$$P_{DC} = \eta_{MPPT} P_{mpp} \tag{5}$$

$$P_{AC} = P_{DC} - \left(P_0 + c_L \cdot P_{AC} + c_Q \cdot P_{AC}^2\right) \tag{6}$$

where P_0 is the no-load power losses along the operation, c_L and c_Q are the linear and quadratic loss coefficients, respectively. The corresponding numerical values are indicated in Table I. For the calculations indicated above, the entries T_{amb}, G_{tcell} and w_s are taken from the forecasts and used to determine the AC power P_{AC}.

To check the accuracy of the PV power conversion model, the measurements of in-plane irradiance G_{tcell}, ambient temperature T_{amb}, and wind speed w_s are used as inputs to the above-described model. Then, the power delivered to the grid, as the main output, can be compared with the energy-meter readings of the PV plant. Thanks to a statistical analysis including only the periods of correct operation of the inverters [35], the average value of the deviations is ≈6% in July, and ≈4% on an annual basis.

III. MODEL STRUCTURE

The underlying assumption in an AR model is that a linear combination of the previous values of a system can be

used to model its output variable. One can generalize this approach to deal with multivariate time series. Let's assume that there are measurements from P output variables ($p = 1, 2, \ldots, P$) (e.g., solar irradiance at particular weather station). These output variables might be measurements of V variables ($v = 1, 2, \ldots, V$) recorded at S locations ($s = 1, 2, \ldots, S$), where $P = V \times S$. Define $y_t^{s,v}$ as the measured value of the v-th variable at the s-th location at time t ($t = 1, 2, \ldots, M + n$). Let y^{v^*,s^*} be any target output variable. A Multivariate Autoregressive (M-AR) is written as

$$y_t^{v^*,s^*} = \sum_{\substack{v=1 \\ s=1}}^{V,S} \sum_{i=1}^{n} y_{t-i}^{v,s} x_i^{v,s} + e_t^{v^*,s^*}, \tag{7}$$

where n is the order, $x_i^{v,s}$ ($\forall i, v, s$) are the regression coefficients, and $e_t^{v^*,s^*}$ is the noise component (usually assumed Gaussian).

Let $N := nP$. Expand (7) to the framework given in (8), shown at the bottom of the page. The goal of the training stage is to calculate model coefficients $\boldsymbol{x} \in \mathbb{R}^N$ that best explain the observations $\boldsymbol{b} \in \mathbb{R}^M$ and $\boldsymbol{A} \in \mathbb{R}^{M \times N}$, considering the noise component $\boldsymbol{e}$. Apparently and based on (8), the coefficients of $\boldsymbol{x}$ are gathered in a block structure. In other words, the vector coefficients for each unique variable appear in one vector-block of length n.

IV. Compressive Spatio-Temporal Forecasting (CSTF)

It is evident from the literature that using spatially distributed irradiance data generally improves the accuracy of the temporal forecasts, particularly enabling to detect cloud advection, which is not possible with data from only one location. Contrary to the widely-used approach in the literature in which the number of exogenous locations to be included in the forecasting is chosen by investigating the relationship between the shifted solar irradiance time series of locations with a time-lagged correlation analysis, it is assumed in this study that only a few meteorological stations, among all stations, have a significant correlation with any given meteorological station. Such relational patterns have been also observed and exploited in wind speed forecasting [36]. Under the assumption of *sparsity* of the interconnections, therefore, $\boldsymbol{x}$ has a particular shape. Precisely, $\boldsymbol{x}$ has a few non-zero entries gathered in few blocks. This structure is known as *block-sparse*. The number of these non-zero blocks equals to the number of stations that significantly contribute to the output in the corresponding time period. The proposed Compressive Spatio-Temporal Forecasting (CSTF) method has the capability of changing the number of non-zero blocks and the value of the coefficients in these blocks for each prediction time horizon. For instance, data from only reference location might be used for a certain prediction period for higher accuracy. Hence, the proposed model behaves like a temporal model, if no reasonable correlations are observed between the reference location and other locations in the previous prediction time. For any given station, the following optimization can be performed in order to obtain the desired $\boldsymbol{x}$ vector:

$$\min_{\boldsymbol{x}} \|\boldsymbol{b} - \boldsymbol{A}\boldsymbol{x}\|_2 \quad \text{subject to} \quad (\boldsymbol{x} \text{ is block-sparse}). \tag{9}$$

A. Background on Compressive Sensing (CS)

Under the assumption of signal sparsity and under given conditions on matrix $\boldsymbol{A}$ [37], CS enables the recovery of a signal from its underdetermined measurement set. A vector of length N with K non-zero entries is called K-sparse where $K < N$. CS provides algorithms for recovery of such vector from its measurements $\boldsymbol{b} = \boldsymbol{A}\boldsymbol{x} \in \mathbb{R}^M$. The matrix $\boldsymbol{A} \in \mathbb{R}^{M \times N}$ is called the measurement matrix with $M < N$. Apparently, there exist many possible solutions to the underdetermined equation $\boldsymbol{b} = \boldsymbol{A}\boldsymbol{x}$; however, if only one solution is suitably sparse, CS algorithms are guaranteed to recover that solution under some specific conditions on $\boldsymbol{A}$. Several recovery guarantees have been proposed in the CS literature. The Restricted Isometry Property (RIP) [38], the Exact Recovery Condition (ERC), and mutual coherence [39] are among the most important proposed conditions on $\boldsymbol{A}$.

B. Uniform CSTF

Tools from CS are used to recover a block-sparse $\boldsymbol{x}$. Let $\boldsymbol{x} \in \mathbb{R}^N$ be a concatenation of P vector-blocks $\boldsymbol{x}_i \in \mathbb{R}^n$, i.e.,

$$\boldsymbol{x} = [\boldsymbol{x}_1^{\text{tr}} \cdots \boldsymbol{x}_i^{\text{tr}} \cdots \boldsymbol{x}_P^{\text{tr}}]^{\text{tr}}, \tag{10}$$

in which $N = nP$. A vector $\boldsymbol{x} \in \mathbb{R}^N$ is called *block K-sparse* if it has $K < P$ non-zero blocks. Among the various extensions of the conventional CS tools, the Block Orthogonal Matching

$$\underbrace{\begin{bmatrix} y_{n+1}^{v^\star,s^\star} \\ y_{n+2}^{v^\star,s^\star} \\ \vdots \\ y_{n+M}^{v^\star,s^\star} \end{bmatrix}}_{\boldsymbol{b} \in \mathbb{R}^M} = \underbrace{\left[\begin{array}{ccc|c|ccc} y_n^{1,1} & \cdots & y_1^{1,1} & \cdots \cdots & y_n^{V,S} & \cdots & y_1^{V,S} \\ y_{n+1}^{1,1} & \ddots & \vdots & & y_{n+1}^{V,S} & \ddots & \vdots \\ \vdots & \ddots & \vdots & & \vdots & \cdots & \vdots \\ y_{n+M-1}^{1,1} & \cdots & y_M^{1,1} & \cdots \cdots & y_{n+M-1}^{V,S} & \cdots & y_M^{V,S} \end{array}\right]}_{\boldsymbol{A} \in \mathbb{R}^{M \times N}} \underbrace{\left[\begin{array}{c} x_1^{1,1} \\ \vdots \\ x_n^{1,1} \\ \hline \vdots \\ \vdots \\ \hline x_1^{V,S} \\ \vdots \\ x_n^{V,S} \end{array}\right]}_{\boldsymbol{x} \in \mathbb{R}^N} \begin{array}{l} \left.\begin{array}{c} \\ \\ \\ \end{array}\right\} \text{Block 1} \\ \\ \\ \left.\begin{array}{c} \\ \\ \\ \end{array}\right\} \text{Block P} \end{array} + \underbrace{\begin{bmatrix} e_{n+1}^{v^\star,s^\star} \\ e_{n+2}^{v^\star,s^\star} \\ \vdots \\ e_{n+M}^{v^\star,s^\star} \end{bmatrix}}_{\boldsymbol{e} \in \mathbb{R}^M} \tag{8}$$

Algorithm 1. The BOMP algorithm for block-sparse recovery

Require: $\boldsymbol{A}$, $\boldsymbol{b}$, $\{n_i\}_{i=1}^{P}$, stopping criteria
Ensure: $\boldsymbol{r}^0 = \boldsymbol{b}$, $\boldsymbol{x}^0 = \boldsymbol{0}$, $\Lambda^0 = \emptyset$, $l = 0$
repeat
1. match: $\boldsymbol{h}_i = \boldsymbol{A}_i^{\text{tr}} \boldsymbol{r}^l$, $i = 1, 2, \cdots, P$
2. identify support: $\lambda = \arg\max_i \|\boldsymbol{h}_i\|_2$
3. update the support: $\Lambda^{l+1} = \Lambda^l \cup \lambda$
4. update signal estimate:
$\boldsymbol{x}^{l+1} = \arg\min_{\boldsymbol{s}:\text{supp}(\boldsymbol{s}) \subseteq \Lambda^{l+1}} \|\boldsymbol{b} - \boldsymbol{A}\boldsymbol{s}\|_2$,
where $\text{supp}(\boldsymbol{s})$ indicates the blocks
on which $\boldsymbol{s}$ may be non-zero
5. update residual estimate: $\boldsymbol{r}^{l+1} = \boldsymbol{b} - \boldsymbol{A}\boldsymbol{x}^{l+1}$
6. increase index l **by** 1
until stopping criteria true
output: $\widehat{\boldsymbol{x}} = \boldsymbol{x}^l = \arg\min_{\boldsymbol{s}:\text{supp}(\boldsymbol{s}) \subseteq \Lambda^l} \|\boldsymbol{b} - \boldsymbol{A}\boldsymbol{s}\|_2$

Pursuit (BOMP) algorithm is used [40], [41]. To find a block-sparse solution to the equation $\boldsymbol{b} = \boldsymbol{A}\boldsymbol{x}$, the formal steps of BOMP are listed in Algorithm 1, where $\boldsymbol{A} \in \mathbb{R}^{M \times N}$ is a concatenation of P matrix-blocks $\boldsymbol{A}_i \in \mathbb{R}^{M \times n}$ ($\forall n_i = n$) as

$$\boldsymbol{A} = [\boldsymbol{A}_1 \cdots \boldsymbol{A}_i \cdots \boldsymbol{A}_P]. \tag{11}$$

Due to the block sparsity of $\boldsymbol{x}$, the vector of observations $\boldsymbol{b}$ can be given as a combination of the columns of $\boldsymbol{A}$, with the selections of the columns occurring in clusters. BOMP aims to determine the participating indices by correlating the $\boldsymbol{b}$ against the columns of $\boldsymbol{A}$ and comparing the correlations among different blocks. When a significant block has been identified, its influence is removed from $\boldsymbol{b}$ and the correlations are recalculated for the remaining blocks. This process repeats until the residual equals zero [41].

C. Nonuniform CSTF

In a uniform CSTF, the assumption is that a meteorological station and the stations in its vicinity can be modeled using AR models of the same order. A more generalized CSTF algorithm is presented in this section, where the AR models of different orders are considered. This algorithm distinguishes between the meteorological stations with different cross-correlation levels with the target station. Let n_i be the order for the i-th station for $i = 1, 2, \ldots, P$. An Nonuniform Multivariate Autoregressive (NM-AR) version of (8) can be written as shown in (12), shown at the bottom of the page, where $n_{\max} \geq \max_i n_i$ and $N := \sum_{i=1}^{P} n_i$. This model structure results in a block-sparse vector with blocks of different length. Let $\boldsymbol{x} \in \mathbb{R}^N$ as a concatenation of P vector-blocks $\boldsymbol{x}_i \in \mathbb{R}^{n_i}$ where $N = \sum_{i=1}^{P} n_i$.

Given $\{n_i\}_{i=1}^{P}$, the BOMP Algorithm 1 can be employed for the recovery of $\boldsymbol{x}$ with $\boldsymbol{A}_i \in \mathbb{R}^{M \times n_i}$. With the objective of finding the set of order $\{n_i\}_{i=1}^{P}$, a correlation analysis is used in which the correlation coefficients for the consecutive time lags up to the prediction horizon between the target and other meteorological stations are calculated. Then the orders accomplishing the best forecasting performance are adjusted considering the calculated correlation coefficients and assigning numbers to the order of each variable of each station proportional to the magnitude of its correlation.

V. Case Study of Five Meteorological Stations in Italy

In this section, the proposed CSTF algorithm is applied by considering G_{tcell}, T_{amb} and w_s measured at five locations in Italy. These locations are suitable choices as: (i) solar irradiance trends exhibit relatively high values and (ii) the stations are located at mutual distances, from about 5 km to about 140 km, making it interesting to consider correlated data.

A. Data Description

Data averaged each 15 min, gathered from five meteorological stations in Italy including Ga1, Ga2, Gi, Ma and Ru, are used in the study. The simulations are carried out for three variables including G_{tcell}, T_{amb} and w_s for whole year 2012; however, the forecasting results are presented for the irradiance data only, which is the most influencing variable on the power calculations, in order to avoid data redundancy. Also, the forecasting results are shown for the target station Gi for two different representative time periods to observe the prediction performance clearly; one in the winter season from February 1, 2012 to February 7, 2012 and the other in the summer season from July 1, 2012 to July 7, 2012 (a period of 7 days). For these periods, training subsets from 11th day of the previous

$$\underbrace{\begin{bmatrix} y_{n_{\max}+1}^{v^\star,s^\star} \\ y_{n_{\max}+2}^{v^\star,s^\star} \\ \vdots \\ y_{n_{\max}+M}^{v^\star,s^\star} \end{bmatrix}}_{\boldsymbol{b} \in \mathbb{R}^M} = \underbrace{\left[\begin{array}{ccccc|c|ccc} y_{n_{\max}}^{1,1} & \cdots & \cdots & \cdots & y_{n_{\max}-n_1+1}^{1,1} & \cdots & y_{n_{\max}}^{V,S} & \cdots & y_{n_{\max}-n_P+1}^{V,S} \\ y_{n_{\max}+1}^{1,1} & \ddots & \ddots & \ddots & \vdots & & y_{n_{\max}+1}^{V,S} & \ddots & \vdots \\ \vdots & \ddots & \ddots & \ddots & \vdots & & \vdots & \ddots & \vdots \\ y_{n_{\max}+M-1}^{1,1} & \cdots & \cdots & \cdots & y_{n_{\max}-n_1+M}^{1,1} & \cdots & y_{n_{\max}+M-1}^{V,S} & \cdots & y_{n_{\max}-n_P+M}^{V,S} \end{array}\right]}_{\boldsymbol{A} \in \mathbb{R}^{M \times N}} \underbrace{\left[\begin{array}{c} x_1^{1,1} \\ \vdots \\ \vdots \\ \vdots \\ x_{n_1}^{1,1} \\ \hline \vdots \\ \hline x_1^{V,S} \\ \vdots \\ x_{n_P}^{V,S} \end{array}\right]}_{\boldsymbol{x} \in \mathbb{R}^N} \begin{array}{l} \left.\begin{array}{c} \\ \\ \\ \\ \end{array}\right\} \text{Block 1} \\ \\ \left.\begin{array}{c} \\ \\ \\ \end{array}\right\} \text{Block P} \end{array} + \underbrace{\begin{bmatrix} e_{n_{\max}+1}^{v^\star,s^\star} \\ e_{n_{\max}+2}^{v^\star,s^\star} \\ \vdots \\ e_{n_{\max}+M}^{v^\star,s^\star} \end{bmatrix}}_{\boldsymbol{e} \in \mathbb{R}^M} \tag{12}$$

month (i.e., January and June, respectively) to the 24th day (a period of 14 days) and model selection subsets from 25th day of the previous month to the 31st day (a period of seven days) are considered.

B. Comparison With the Benchmark Methods

For temporal forecasting, the *persistence* model is used as the first choice. In persistence model the last measurement is used as the next forecast. It is worth noting that the relatively short forecast horizon (three hours) adopted in this study makes persistence method a good candidate as a benchmark model for solar irradiance forecasts [42], [43] since this method gives very reasonable results for particularly short terms [44]. Furthermore, in order to increase the efficiency of persistence model as well as other approaches, the irradiance data are divided into two subsets, i.e., daytime and nighttime, and only the daytime data are used in the forecasting process while the nighttime data are assumed to be zero. For the purpose of choosing the start and end times of daylight, the corresponding values belonging to the last day of model selection subset are adopted and these times are kept constant during the next prediction horizon.

Also an AR model is considered, in which the optimal order values are obtained using the model selection subset. In the forecasting stage, multi-step predictions are carried out in a recursive manner for seven consecutive days with three hour-ahead updates. In other words, each forecasted value is used in the next consecutive forecast; the input data set is also updated at every prediction horizon, both of these help the model exhibit the latest trend of irradiance profile. The results for these models are given in Figs. 2 and 3, respectively. As can be seen, the persistence method gives values which remain constant at the time of forecast. These are appeared as step changes in solar irradiance at the beginning of each forecast. Due to the "quasi-stationary" characteristic of solar irradiance in each three-hour period, reasonable forecasts are achieved with such a simple method. Then, including a number of recent values in the considered AR model enables higher-accuracy forecasts compared to the persistence model.

A forecasting approach combining Wavelet Decomposition and Neural Network (NN) is also presented for comparisons. In this model, the solar irradiance series is decomposed by the Wavelet Transform (WT) into a given number of components at different frequency bands. Forecast of each band is then performed simultaneously employing the ANN method and final forecast is obtained with the aggregation of these individual forecasts (see [45] for further details). As seen from Fig. 4, the combined model outperforms the AR model due to its capability of modeling the nonlinearity in the irradiance data.

In addition to the basic temporal models, two methods based on spatial information are employed in the comparisons. The first model, which is proposed Bilgili et al. [46], applies the solar irradiance data from the five stations to an ANN model. The latter model uses Least Squares (LS) method to calculate the coefficients of an M-AR model. Including spatial information enhances the prediction accuracy compared to the temporal models, as shown in Figs. 5 and 6.

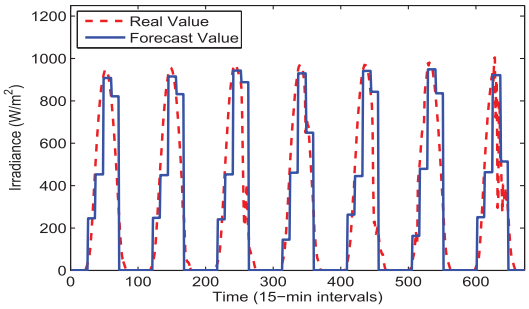

(a) Summer

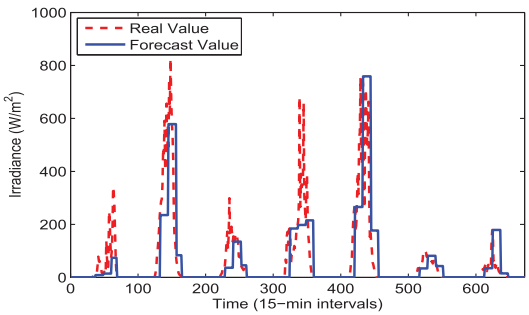

(b) Winter

Fig. 2. Persistence forecasting of two data sets.

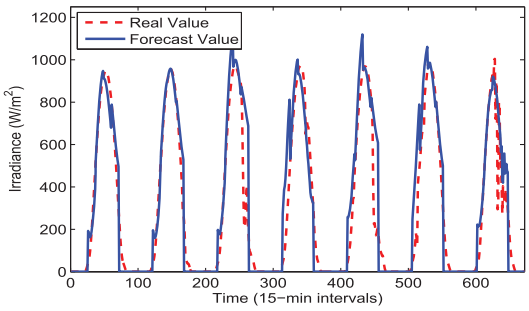

(a) Summer

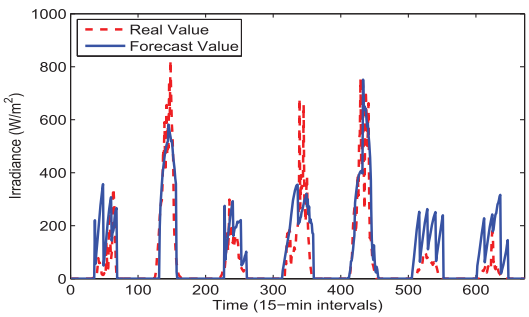

(b) Winter

Fig. 3. AR forecasting of two data sets.

C. Nonuniform CSTF

The nonuniform CSTF algorithm is then applied. The considered prediction time horizon is 3 hours in the simulations, thus a vector $\boldsymbol{x}$ is calculated every 12 steps as each step is 15 minutes. A recursive approach is adopted in the predictions. The solar irradiance forecasts at time $n + M + 1$ for the stations

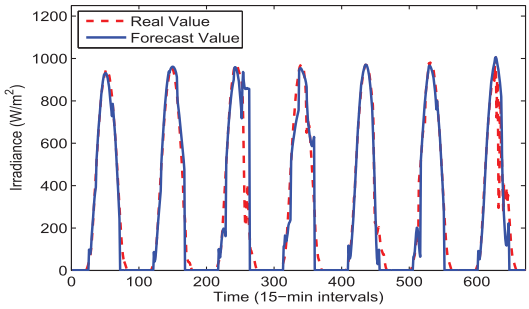

(a) Summer

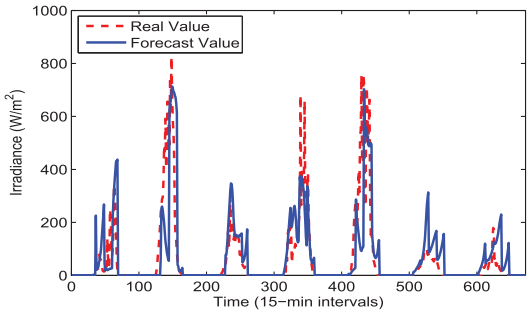

(b) Winter

Fig. 4. WT-ANN forecasting of two data sets.

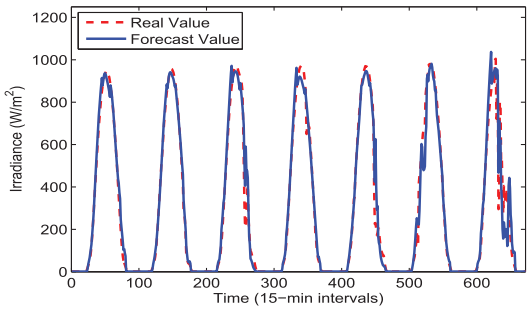

(a) Summer

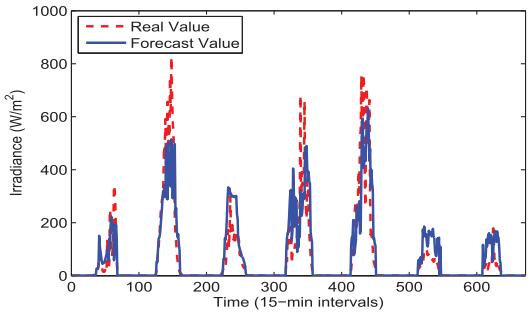

(b) Winter

Fig. 5. Multi-input NN forecasting of two data sets.

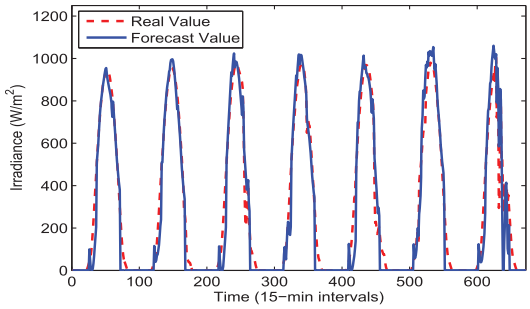

(a) Summer

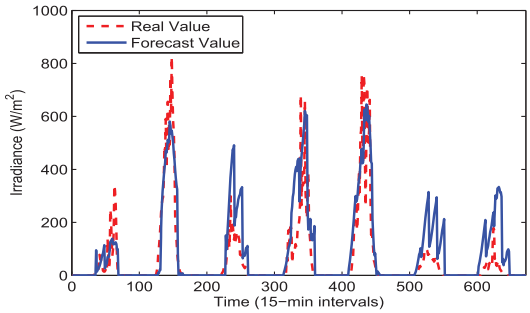

(b) Winter

Fig. 6. LS M-AR forecasting of two data sets.

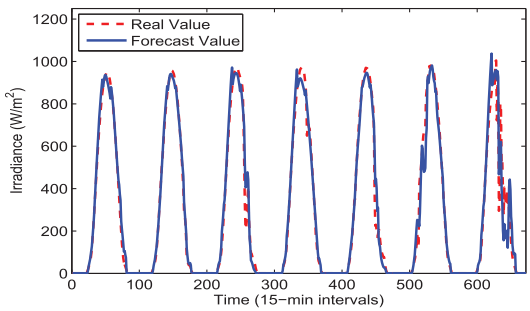

(a) Summer

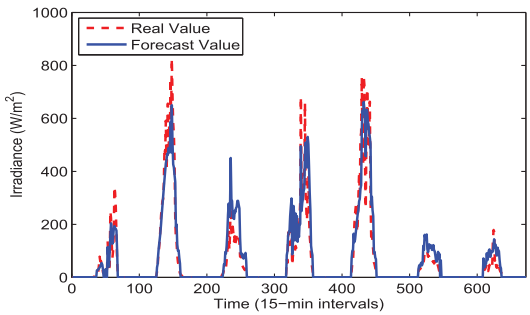

(b) Winter

Fig. 7. Nonuniform CSTF forecasting of two data sets.

$(\hat{y}^i_{n+M+1}, \forall i)$ are included in $\boldsymbol{A}$ for forecasting the solar irradiance at time $n+M+2$ $(\hat{y}^i_{n+M+2}, \forall i)$. This process continues for 12 steps while entries of $\boldsymbol{A}$ are continuously changed with the observations for each prediction time.

The prediction accuracy is substantially improved compared to the temporal and spatio-temporal benchmark models for both data sets, as shown in Fig. 7. In order to clearly observe the superiority of the proposed model, the two widely-used error metrics are presented for the solar prediction methods considered in this study for the whole year 2012 in Table II. Mean Absolute Error (MAE) gives the mean of the absolute value of the deviation between the real and forecasted data, and Root Mean Squared Error (RMSE) assigns a higher weight to large error values by squaring them. Moreover, the Normalized Root

TABLE II
ERROR METRICS OF DIFFERENT METHODS FOR THE WHOLE YEAR 2012

Forecasting Approach	MAE $[W/m^2]$	RMSE $[W/m^2]$	NRMSE [%]	Forecast skill
Persistence Forecasting	87.29	167.22	14.45	0
AR	69.11	132.38	11.44	0.21
WT-ANN	58.29	111.67	9.65	0.33
Multi-input ANN	57.71	109.12	9.43	0.35
LS-based ST	55.94	107.16	9.26	0.36
Nonuniform CSTF	39.98	77.76	6.72	0.53

Mean Squared Error (NRMSE) is provided to present a scale-independent error metric. Note that the considered error measures are negatively oriented and the smaller the values are, the better the forecast is. Evidently, the proposed nonuniform CSTF method outperforms other approaches tested. Considering the NRMSE, the nonuniform CSTF approach provides a reduction of 53%, 41% and 30% compared to the persistence, AR, and WT-ANN models, respectively, and a reduction of 27% compared to the LS-based ST model. Table II also shows the *forecast skill*, which represents the forecast error obtained by relating the forecast accuracy of the models to that of the persistence model. A forecast skill of 1.0 implies an unattainable perfect forecasting, and a forecast skill of 0.0 indicates a performance similar to the persistence method. Besides, negative values show lower forecasting accuracies compared to the persistence method. Detailed explanations and applications of the forecast skill can be found in Ref. [47].

Note that various variables apart from the target variable are incorporated in the LS M-AR model and in the proposed model. The type of the exogenous variables to be included as an input is determined by analyzing the cross-correlations between the target variable and other variables in the training stage. If the correlation exceeds a threshold value for a given variable, this variable is included in the input data set in order to increase the forecasting accuracy. With this objective, temperature and humidity values are used for irradiance forecasts in addition to irradiance data in order to take advantage of high correlations between these variables. Also, irradiance, humidity and wind direction are considered for temperature forecasts while temperature and wind direction series are included in wind speed forecasts. Moreover, the order of each variable is chosen in the model selection stage by analyzing the cross-correlations and comparing the results obtained for different order values. In other words, the order values are calculated based on the correlation coefficients and then fine-tuned by trial and error method through experiments. It is important to state that the type and order of the variables are determined once in the training and model selection stages and then kept constant during the test periods.

Figure 8 shows the coefficient vectors for the proposed method at the training stage for both seasons. As seen, only a few blocks are non-zero in each season, resulting in a block-sparse $\boldsymbol{x}$. In other words, only some of the variables from some stations are dominant for the given period. As an example, it can be observed from Fig. 8 that the most contributing data in the forecasts of the first three-hour period for both seasons is the irradiance data taken from target meteorological station

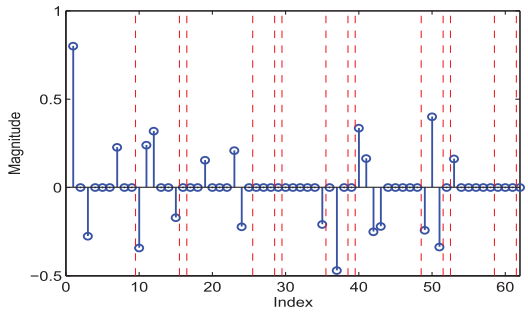

(a) Summer

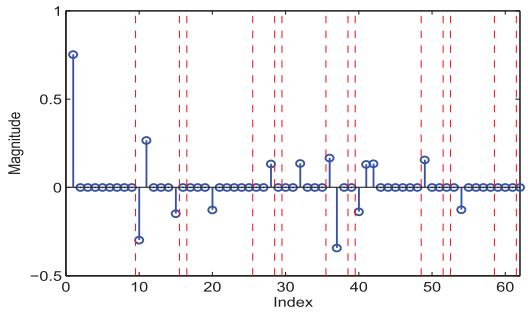

(b) Winter

Fig. 8. The coefficient vector at the training stage. The red dashed lines define 15 vector-blocks (three variables from five meteorological stations) of the coefficient vector.

at time $t-1$ (the first blue solid line), which has a magnitude of over 0.7 for both cases. It is obvious that these high magnitudes are the result of the very high correlation between the consecutive values of the same variable, which is also consistent with the main idea of persistence and AR models. The humidity measurement from station Ru at time $t-1$, which corresponds to the zero value in the rightmost blocks in Fig. 8, on the contrary, does not make a contribution to the forecasts in the related periods. It can be highlighted that the contribution level of each variable from different stations is first determined considering the correlation between the target variable and all the available data in the training and model selection stages. The block-sparse structure (i.e., the location and magnitude of non-zero blocks) is changed slightly in the subsequent coefficient vectors.

The CSTF model has a relatively short computational time, taking about 0.6 seconds for each 12 steps in the MATLAB environment on a 2.0 GHz, quad-core i7 processor PC with 8GB of RAM. Compared to the benchmark methods used in this paper, for instance, this time is almost half of the time required by the WT-ANN model to get comparable prediction accuracy. It is noted that in addition to the forecasts of irradiance, ambient temperature and wind speed, the proposed approach can be used effectively for a wide range of short-term forecasting applications, including wind direction, rainfall, electric load demand and even urban and highway traffic volumes, thanks to its very flexible structure and fast response time. The existing strong correlations between the time series of such measurements in both spatial and temporal dimensions would help the proposed algorithm improve the

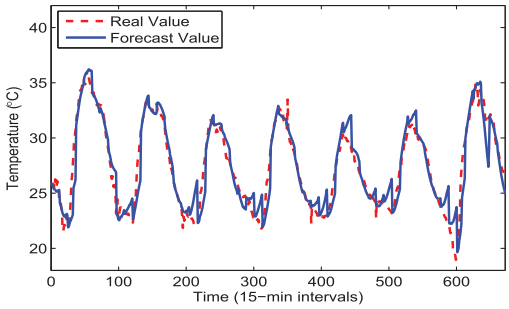

(a) Summer

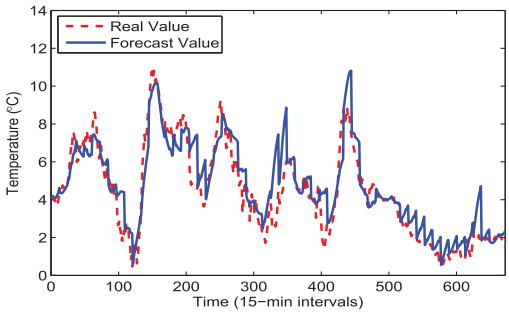

(b) Winter

Fig. 9. Nonuniform CSTF forecasting of two temperature data sets.

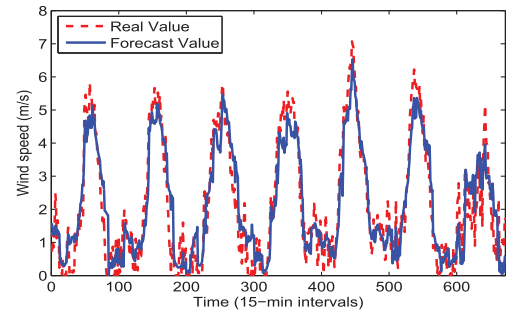

(a) Summer

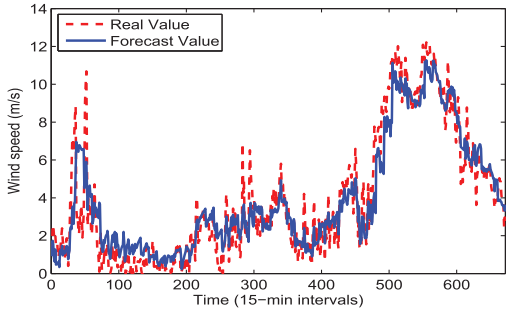

(b) Winter

Fig. 10. Nonuniform CSTF forecasting of two wind speed data sets.

related forecasts without increasing the computational burden, as in the results presented in this paper.

D. PV Power Predictions

Similar to the irradiance forecasts, ambient temperature and wind speed are also forecasted with the proposed forecasting algorithm with some modifications, as shown in Figs. 9 and 10. The error metrics for these variables are given in Table III. Lastly, the predicted data of all three variables are applied to the power conversion model in order to estimate the output power produced by the PV plant. As seen from Fig. 11, the forecasted values are mostly consistent with the real data. The calculated error measures for power, shown in Table III, validate the effectiveness of the proposed models, which comes from exploiting all available data in an optimum manner.

TABLE III
STATISTICAL ERROR MEASURE OF OTHER VARIABLES AND POWER FOR THE WHOLE YEAR 2012

Forecasted Variable	MAE	RMSE	NRMSE [%]	Forecast Skill
Temperature	1.31 [°C]	1.51 [°C]	3.81	0.18
Wind Speed	1.27 [m/s]	1.01 [m/s]	6.88	0.29
Power	27.68 [kW]	76.98 [kW]	6.61	0.55

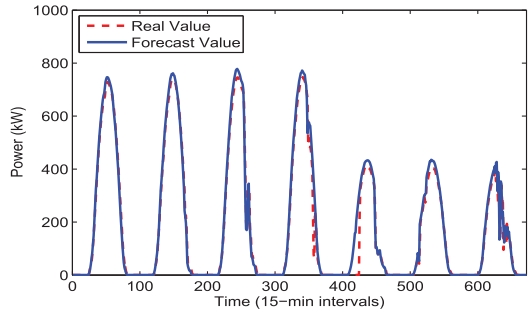

(a) Summer

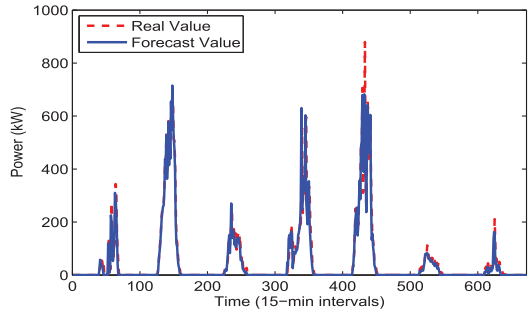

(b) Winter

Fig. 11. Nonuniform CSTF forecasting of two power data sets.

VI. CONCLUSION

This study proposes a solar power forecasting scheme which uses spatial and temporal time series data as well as a PV power conversion model. The PV power conversion model uses the forecast of three different variables, namely, irradiance on the tilted plane, ambient temperature and wind speed, in order to estimate the output power produced by a PV plant. The forecast values are obtained with a spatio-temporal forecasting approach that includes data from a target meteorological station and its surrounding stations. The comparison results against a set of benchmark methods show that the CSTF approach significantly increases the accuracy of short-term forecasts. Furthermore, the calculated power forecasts show that the PV power conversion model provides accurate modeling together with the forecasts of above-mentioned three variables. As a future direction, the

effectiveness of the forecasts with a higher number of meteorological stations for especially longer prediction horizons will be investigated. Examining the possible contributions of incorporating the residual prediction errors and/or their forecasts in the proposed model is considered as another future study.

REFERENCES

[1] L. Xie, Y. Gu, X. Zhu, and M. G. Genton, "Short-term spatio-temporal wind power forecast in robust look-ahead power system dispatch," *IEEE Trans. Smart Grid*, vol. 5, no. 1, pp. 511–520, 2014.

[2] R. Bessa, A. Trindade, and V. Miranda, "Spatial-temporal solar power forecasting for smart grids," *IEEE Trans. Ind. Informat.*, vol. 11, no. 1, pp. 232–241, Feb. 2015.

[3] A. Tascikaraoglu and M. Uzunoglu, "A review of combined approaches for prediction of short-term wind speed and power," *Renew. Sustain. Energy Rev.*, vol. 34, pp. 243–254, 2014.

[4] M. He, L. Yang, J. Zhang, and V. Vittal, "A spatio-temporal analysis approach for short-term forecast of wind farm generation," *IEEE Trans. Power Syst.*, vol. 29, no. 4, pp. 1611–1622, Jul. 2014.

[5] J. Dowell, S. Weiss, D. Hill, and D. Infield, "Short-term spatio-temporal prediction of wind speed and direction," *Wind Energy*, vol. 17, no. 12, pp. 1945–1955, 2014.

[6] J. Dowell and P. Pinson, "Very-short-term probabilistic wind power forecasts by sparse vector autoregression," *IEEE Trans. Smart Grid*, vol. 7, no. 2, pp. 763–770, Mar. 2016.

[7] C. Yang *et al.*, "Multitime-scale data-driven spatio-temporal forecast of photovoltaic generation," *IEEE Trans. Sustain. Energy*, vol. 6, no. 1, pp. 104–112, Jan. 2015.

[8] V. P. Lonij, A. E. Brooks, A. D. Cronin, M. Leuthold, and K. Koch, "Intra-hour forecasts of solar power production using measurements from a network of irradiance sensors," *Solar Energy*, vol. 97, pp. 58–66, 2013.

[9] D. Yang, C. Gu, Z. Dong, P. Jirutitijaroen, N. Chen, and W. M. Walsh, "Solar irradiance forecasting using spatial-temporal covariance structures and time-forward kriging," *Renew. Energy*, vol. 60, pp. 235–245, 2013.

[10] R. Dambreville, P. Blanc, J. Chanussot, and D. Boldo, "Very short term forecasting of the global horizontal irradiance using a spatio-temporal autoregressive model," *Renew. Energy*, vol. 72, pp. 291–300, 2014.

[11] G. Licciardi, R. Dambreville, J. Chanussot, and S. Dubost, "Spatiotemporal pattern recognition and nonlinear PCA for global horizontal irradiance forecasting," *Geosci. Remote Sens. Lett.*, vol. 12, pp. 284–288, 2015.

[12] A. Zagouras, H. T. Pedro, and C. F. Coimbra, "On the role of lagged exogenous variables and spatio–temporal correlations in improving the accuracy of solar forecasting methods," *Renew. Energy*, vol. 78, pp. 203–218, 2015.

[13] D. Yang, Z. Ye, L. H. I. Lim, and Z. Dong, "Very short term irradiance forecasting using the lasso," *Solar Energy*, vol. 114, pp. 314–326, 2015.

[14] A. W. Aryaputera, D. Yang, L. Zhao, and W. M. Walsh, "Very short-term irradiance forecasting at unobserved locations using spatio-temporal kriging," *Solar Energy*, vol. 122, pp. 1266–1278, 2015.

[15] D. Yang, Z. Dong, T. Reindl, P. Jirutitijaroen, and W. M. Walsh, "Solar irradiance forecasting using spatio-temporal empirical kriging and vector autoregressive models with parameter shrinkage," *Solar Energy*, vol. 103, pp. 550–562, 2014.

[16] D. S. Callaway and M. D. Tabone, "Modeling variability and uncertainty of photovoltaic generation: A hidden state spatial statistical approach," *IEEE Trans. Power Syst.*, vol. 30, no. 6, pp. 2965–2973, Nov. 2015.

[17] J. E. B. Iversen and P. Pinson, "Resgen: Renewable energy scenario generation platform," in *Proc. IEEE PES Gen. Meeting*, 2016, to be published.

[18] J. Boland, "Spatial-temporal forecasting of solar radiation," *Renew. Energy*, vol. 75, pp. 607–616, 2015.

[19] M. Diagne, M. David, P. Lauret, J. Boland, and N. Schmutz, "Review of solar irradiance forecasting methods and a proposition for small-scale insular grids," *Renew. Sustain. Energy Rev.*, vol. 27, pp. 65–76, 2013.

[20] J. Zeng and W. Qiao, "Short-term solar power prediction using a support vector machine," *Renew. Energy*, vol. 52, pp. 118–127, 2013.

[21] P. Mathiesen, J. M. Brown, and J. Kleissl, "Geostrophic wind dependent probabilistic irradiance forecasts for coastal california," *IEEE Trans. Sustain. Energy*, vol. 4, no. 2, pp. 510–518, Apr. 2013.

[22] Y. Chu, H. T. Pedro, M. Li, and C. F. Coimbra, "Real-time forecasting of solar irradiance ramps with smart image processing," *Solar Energy*, vol. 114, pp. 91–104, 2015.

[23] V. Cocina, "Economy of grid-connected photovoltaic systems and comparison of irradiance / electric power predictions vs. experimental results," Ph.D. dissertation, Politecnico di Torino, Italy, 2014.

[24] F. Spertino, P. Di Leo, and V. Cocina, "Accurate measurements of solar irradiance for evaluation of photovoltaic power profiles," in *Proc. IEEE Grenoble PowerTech (POWERTECH'13)*, Grenoble, France, Jun. 16–20, 2013.

[25] A. Reinders, V. Van Dijk, E. Wiemken, and W. Turkenburg, "Technical and economic analysis of grid-connected PV systems by means of simulation," *Progr. Photovoltaics*, vol. 7, pp. 71–82, 1999.

[26] M. Gostein, J. R. Caron, and B. Littmann, "Measuring soiling losses at utility-scale PV power plants," in *Proc. 40th IEEE Photovoltaic Spec. Conf. (PVSC'14)*, 2014, pp. 0885–0890.

[27] Joint Research Centre of the European Commission. *Photovoltaic geographical information system (PVGIS)* [Online]. Available: http://re.jrc.ec.europa.eu/pvgis/apps4/pvest.php =0pt

[28] F. Spertino, F. Corona, and P. Di Leo, "Limits of advisability for master–slave configuration of DC–AC converters in photovoltaic systems," *IEEE J. Photovoltaics*, vol. 2, no. 4, pp. 547–554, Oct. 2012.

[29] T. Markvart, *Solar Electricity*. Hoboken, NJ, USA Wiley, 2000, vol. 6.

[30] IEC, Crystalline Silicon Photovoltaic (PV) Array. On-Site Measurement of I-V Characteristics, International Standard IEC 61829, 1998.

[31] G. TamizhMani, L. Ji, Y. Tang, L. Petacci, and C. Osterwald, "Photovoltaic module thermal/wind performance: Long-term monitoring and model development for energy rating," in *Proc. NCPV Solar Program Rev. Meeting*, 2003, pp. 936–939, [Online]. Available: http://www.nrel.gov/docs/fy03osti/35645.pdf. Accessed on: Jan. 15, 2016.

[32] R. Chenni, M. Makhlouf, T. Kerbache, and A. Bouzid, "A detailed modeling method for photovoltaic cells," *Energy*, vol. 32, no. 9, pp. 1724–1730, 2007.

[33] F. Spertino and J. Sumaili Akilimali, "Are manufacturing I-V mismatch and reverse currents key factors in large photovoltaic arrays?" *IEEE Trans. Ind. Electron.*, vol. 56, no. 11, pp. 4520–4531, Nov. 2009.

[34] F. Spertino and F. Corona, "Monitoring and checking of performance in photovoltaic plants: A tool for design, installation and maintenance of grid-connected systems," *Renew. Energy*, vol. 60, pp. 722–732, 2013.

[35] G. Chicco, V. Cocina, P. Di Leo, and F. Spertino, "Weather forecast-based power predictions and experimental results from photovoltaic systems," in *Proc. IEEE Int. Symp. Power Electron. Elect. Drives Autom. Motion (SPEEDAM'14)*, 2014, pp. 342–346.

[36] B. M. Sanandaji, A. Tascikaraoglu, K. Poolla, and P. Varaiya, "Low-dimensional models in spatio-temporal wind speed forecasting," in *Proc. Amer. Control Conf. (ACC'15)*, 2015, pp. 4485–4490.

[37] D. L. Donoho, "Compressed sensing," *IEEE Trans. Inf. Theory*, vol. 52, no. 4, pp. 1289–1306, Apr. 2006.

[38] E. Candès, "The restricted isometry property and its implications for compressed sensing," *Comptes rendus-Mathématique*, vol. 346, no. 9–10, pp. 589–592, 2008.

[39] J. Tropp, "Greed is good: Algorithmic results for sparse approximation," *IEEE Trans. Inf. Theory*, vol. 50, no. 10, pp. 2231–2242, Oct. 2004.

[40] B. M. Sanandaji, T. L. Vincent, and M. B. Wakin, "Compressive topology identification of interconnected dynamic systems via clustered orthogonal matching pursuit," in *Proc. 50th IEEE Conf. Decis. Control*, 2011, pp. 174–180.

[41] B. M. Sanandaji, T. L. Vincent, and M. B. Wakin, "A review of sufficient conditions for structure identification in interconnected systems," in *Proc. 16th IFAC Symp. Syst. Identif.*, 2012, pp. 1623–1628.

[42] C. Voyant, C. Darras, M. Muselli, C. Paoli, M.-L. Nivet, and P. Poggi, "Bayesian rules and stochastic models for high accuracy prediction of solar radiation," *Appl. Energy*, vol. 114, pp. 218–226, 2014.

[43] E. W. Law, A. A. Prasad, M. Kay, and R. A. Taylor, "Direct normal irradiance forecasting and its application to concentrated solar thermal output forecasting–a review," *Solar Energy*, vol. 108, pp. 287–307, 2014.

[44] A. Tascikaraoglu, A. Boynuegri, and M. Uzunoglu, "A demand side management strategy based on forecasting of residential renewable sources: A smart home system in turkey," *Energy Build.*, vol. 80, pp. 309–320, 2014.

[45] A. Tascikaraoglu, M. Uzunoglu, and B. Vural, "The assessment of the contribution of short-term wind power predictions to the efficiency of stand-alone hybrid systems," *Appl. Energy*, vol. 94, pp. 156–165, 2012.

[46] M. Bilgili, B. Sahin, and A. Yasar, "Application of artificial neural networks for the wind speed prediction of target station using reference stations data," *Renew. Energy*, vol. 32, no. 14, pp. 2350–2360, 2007.

[47] R. H. Inman, H. T. Pedro, and C. F. Coimbra, "Solar forecasting methods for renewable energy integration," *Progr. Energy Combust. Sci.*, vol. 39, no. 6, pp. 535–576, 2013.